SYNTHESIS, CRYSTAL STRUCTURE AND STUDY OF THE [Fe(DIPIC)(NO_3)(H_2O)$_2$] COMPLEX COMPOUND

Y.E. Nazarov[a], Kh.Kh. Turaev[a], Sh.A. Kasimov[a], A.K. Nomozov*[b, d, c], A.A. Rasulov[a], Sh.Sh. Ochildiev[a], F.B. Kurbonov[a]

[a]*Faculty of Chemistry, Termez State University, Termez 190111, Uzbekistan*
[b]*Uzbekistan Research Institute of Chemical Technologies in Tashkent, Tashkent Uzbekistan*
[c]*Department of Microbiology and Epidemiology, Termez Branch of Tashkent Medical University, Termez 190111, Uzbekistan*
[d]*Department of Natural Sciences, Termez University of Economics and Service. Termez, Farovon Street 4-b, Surkhandarya, 190111, Uzbekistan*

e-mail: abror_nomozov@tues.uz

Received 02.03.2026
Accepted 23.06.2026

Abstract: *A new iron(III) complex, [Fe(dipic)(NO_3)(H_2O)$_2$], containing the 2,6-pyridinedicarboxylate (dipic) ligand, was synthesized and characterized by single-crystal X-ray diffraction. The crystal structure revealed an octahedral coordination environment around the Fe(III) center, where the dipicolinate ligand coordinates in a tridentate mode together with one nitrate ion and two water molecules. The crystallographic data were deposited in the Cambridge Crystallographic Data Centre (CCDC 2400919). Density functional theory (DFT) calculations were performed using the PBE-D4/def2-TZVP and B3LYP-D4/def2-TZVP methods. The calculated energies indicated that the sextet state represents the most stable electronic configuration of the complex. Frontier molecular orbital and electrostatic potential (ESP) analyses were employed to investigate the electronic structure and reactive sites. Hirshfeld surface analysis showed that the crystal packing is mainly governed by O···H/H···O intermolecular interactions, while void analysis revealed a low free-volume fraction, indicating efficient crystal packing and structural stability. The combined experimental and theoretical results provide valuable insights into the structural and electronic properties of this new iron(III) dipicolinate complex.*

Keywords: *Complex, X-ray structure analysis, Hirshfeld surface analysis, 2,6-pyridinedicarboxylic acid (2,6-PDCA, dipic), ligand, complex, DFT, ESP.*

Introduction

2,6-Pyridincarboxylic acid (2,6-PDCA, dipic) is a versatile N,O-chelating, bidentate and tridentate chelating ligand that forms stable complexes via one or more carboxylate oxygen atoms [1-4]. The reason for the interest is that the ligand has a rigid 120° angle between the H2pda and the central pyridine ring and two carboxylate groups and therefore can provide a variety of binding modes for formation [5].

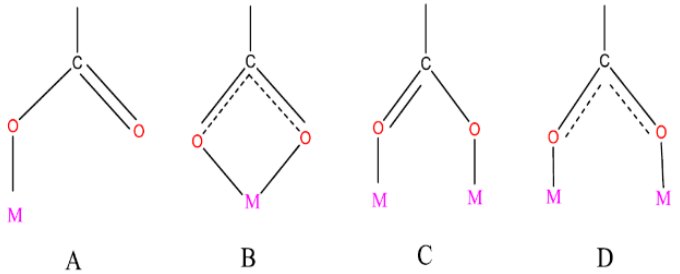


Fig. 1. The bonding of the carboxylate (COO) group to the metal, i.e., asymmetric monodentate (A), symmetric bidentate (B) and asymmetric bidentate (C, D).

Dipicolinic acid (H_2dipic) has attracted considerable attention in coordination chemistry because of its versatile coordination behavior and ability to form stable metal complexes. In addition to acting as a hydrogen-bond donor and acceptor, it exhibits diverse coordination modes, including monodentate, bidentate, tridentate, and bridging forms in its neutral, monoanionic, and dianionic states [6–16]. Owing to these properties, dipicolinate complexes have found applications in medicinal chemistry, analytical chemistry, and bioinorganic studies.

Numerous metal–dipicolinate complexes have been synthesized and structurally characterized, including complexes of Cu, Zn, Mn, Ni, and Fe [17-19]. Among these, iron–dipicolinate complexes are of particular interest because of the biological and chemical importance of iron. Previous studies have reported a variety of Fe(III) complexes containing one or two dipicolinate ligands, in which the metal center commonly adopts a distorted octahedral coordination geometry [20].

Dipicolinic acid is also known for its ability to stabilize unusual oxidation states and its applications in corrosion inhibition, metal-ion determination, and environmental analysis [21-28]. Although Fe(II) salts are frequently used as starting materials, oxidation to Fe(III) often occurs during complex formation, resulting in thermodynamically stable Fe(III) products. Magnetic and Mössbauer spectroscopic studies have shown that bis(dipicolinato)ferrate(III) complexes generally exist in a high-spin state [29,30].

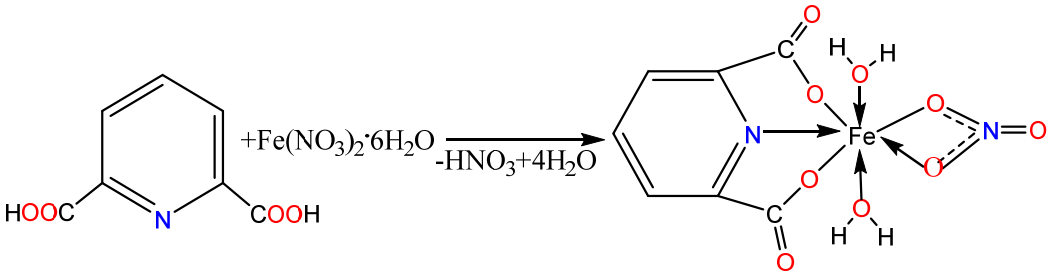
In this work, we present the synthesis, DFT, Hershfeld surface, and ESP analysis of the complex [Fe(dipic))(NO_3)(H_2O)$_2$] Fe(III) with 2,6-pyridinedicarboxylic acid in the presence of $Fe(NO_3)_2{\cdot}6H_2O$.

Experimental Part

Materials and Methods. Iron(II) nitrate hexahydrate, $Fe(NO_3)_2{\cdot}6H_2O$, and 2,6-pyridinedicarboxylic acid (2,6-PDCA) were used as starting materials. All reagents were of analytical grade and were purchased from Merit Chemicals without further purification.

X-ray Structure Determination. The molecular and crystal structure of the synthesized complex was determined by single-crystal X-ray diffraction using an Xcalibur® Oxford Diffraction diffractometer equipped with a graphite monochromator and Cu Kα radiation (λ = 1.54184 Å).

Synthesis of the Complex Compound. Iron(II) nitrate hexahydrate, $Fe(NO_3)_2{\cdot}6H_2O$ (0.288 g, 1 mmol), and 2,6-pyridinedicarboxylic acid (2,6-PDCA, H_2dipic) (0.167 g, 1 mmol) were separately dissolved in distilled water. The resulting solutions were mixed in a 1:1 molar ratio and stirred magnetically at 60 °C for 30 min. The reaction mixture was then allowed to stand at room temperature for crystallization. After 10 days, yellow crystals suitable for single-crystal X-ray diffraction analysis were obtained. Structural analysis revealed the formation of the complex [Fe(dipic)(NO_3)(H_2O)$_2$]. The isolated product was obtained in 76% yield. Anal. Calcd for [Fe(dipic)(NO_3)(H_2O)$_2$] ($C_7H_7FeN_2O_9$, Mr = 344.06): C, 24.41; H, 2.05; N, 8.13; O, 41.85%. Found: C, 24.35; H, 2.01; N, 8.04; O, 41.57%.



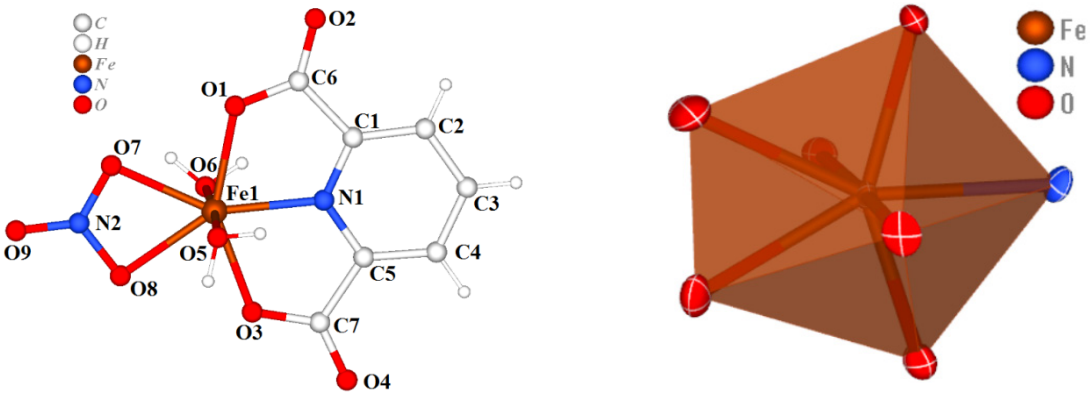
Scheme 1. Synthesis reaction of complex compound [Fe(dipic)(NO_3)(H_2O)$_2$]

Structural Commentary. The complex [Fe(dipic)(NO_3)(H_2O)$_2$] crystallizes in the orthorhombic crystal system with the space group $Pca2_1$. The unit-cell parameters are a = 11.7097(2) Å, b = 9.0760(1) Å, c = 9.8525(2) Å, α = β = γ = 90° (Table 1).

In the crystal structure, the dipicolinate ligand coordinates to the Fe(III) center in a tridentate chelating mode through the pyridine nitrogen atom and two carboxylate oxygen atoms. The coordination sphere is completed by one nitrate ion and two coordinated water molecules, resulting in a distorted octahedral geometry around the metal center.

Table 1. Crystal data of the [Fe(dipic)(NO_3)(H_2O)$_2$] complex

Parameters	**Values**	**Parameters**	**Values**
[Fe(dipic)(NO_3)(H_2O)$_2$]			
Formula	$C_7H_7FeN_2O_9$	Crystal size, mm	0.30 x 0.28 x 0.24
Molecular mass	344.056	Temperature T, °C	293
Syngonia	orthorhombic	Scan interval 0, °	□ = 4.9–71.1°
Spatial group	Pca21	Interval h,k,l	-14: 14; -11: 11; -12: 8
a, Å	11.7097(2)	Tmin, Tmax No. of measured	8976, 1730, 1551
b, Å	9.0760(1)	(sin θ/λ) max (Å−1)	0.614
c, Å	9.8525(2)	R_{int}	0.068
α°	90	Tmin, Tmax	0.463, 1.000
β°	90	No. of reflections	1734
γ°	90	No. of parameters	174
V, Å^3	1047.10(3)	R1, wR2(1>2σ(I))	0.0386, 0.1061, 1.06
Z	5	$\Delta_{pmin/max}$eÅ^{-3}	-1.00, 0.38
D_xg/sm^3	2.023	Theta(max)	71.327
μ(CuKα),m m^{-1}	12.116	CCDC-number	2400919



a **b**

Fig.2. Molecular structure a) and orthorhombic shape b) of the complex [Fe(dipic)(NO_3)(H_2O)$_2$]

Selected bond lengths include Fe1–N1 = 2.078(3) Å, Fe1–O1 = 2.099(5) Å, Fe1–O3 = 2.080(5) Å, Fe1–O5 = 2.030(5) Å, and Fe1–O6 = 2.029(5) Å (Table 2). These values are comparable to those reported for related iron–dipicolinate complexes. For example, in [C_5H_5NH][Fe(dipic)(Hdipic)(C_5H_5N)$_2$], the Fe–N and Fe–O bond lengths are 2.133(2), 2.1614(19), and 2.2095(18) Å, respectively [30]. Similarly, in (NH_4)[Fe(dipic)$_2$], the Fe–N and Fe–O bond distances are 2.0538(13) and 2.0123(8) Å, respectively.

The coordination geometry is further confirmed by the observed bond angles. In particular, the O7–Fe1–N1 angle of 150.7(3)° indicates a distorted octahedral arrangement around the Fe(III) ion (Fig. 2).

Fig. 3 shows the crystal structure of the complex. The dotted lines indicate the molecular and intermolecular hydrogen bonds. Table 3 lists the hydrogen bond geometry.

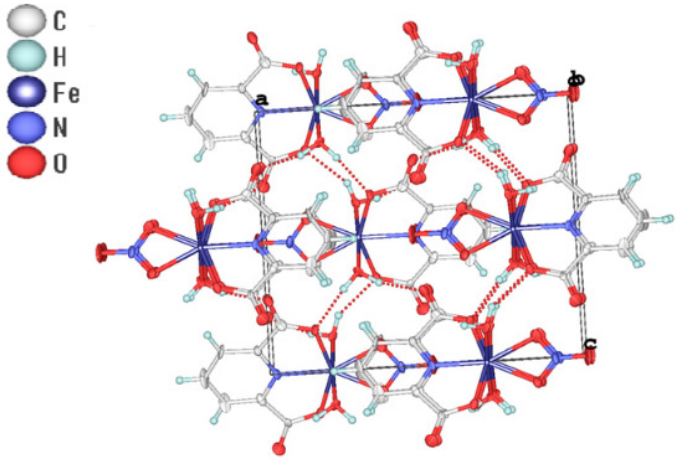


Fig. 3. Crystal structure of the complex. *Dotted lines indicate hydrogen bonds*.

Table 2. Selected bond lengths and bond angles of the [Fe(dipic)(NO_3)(H_2O)$_2$] complex

Bond length	**(Å)**	**Bond angle**	**(°)**
Fe1—O1	2.099 (5)	O1—Fe1—O8	134.67 (19)
Fe1—O5	2.030 (5)	O1—Fe1—O7	75.5 (2)
Fe1—O8	2.142 (5)	O5—Fe1—O1	90.2 (2)
Fe1—O3	2.080 (5)	O5—Fe1—O8	87.10 (19)
Fe1—O6	2.029 (5)	O5—Fe1—O3	91.0 (2)
Fe1—O7	2.161 (5)	O5—Fe1—O7	89.8 (2)
Fe1—N1	2.078 (3)	O5—Fe1—N1	91.7 (2)
O1—C6	1.291 (7)	O8—Fe1—O7	59.23 (10)
O5—H5A	0.8566	O3—Fe1—O1	149.18 (9)
O5—H5B	0.8561	O3—Fe1—O8	76.1 (2)
O8—N2	1.257 (11)	O3—Fe1—O7	135.3 (2)
O3—C7	1.290 (7)	O6—Fe1—O1	89.8 (2)
O6—H6A	0.8527	O6—Fe1—O5	176.83 (12)
O6—H6B	0.8521	O6—Fe1—O8	90.66 (18)
O2—C6	1.223 (9)	O6—Fe1—O3	90.6 (2)
O7—N2	1.290 (11)	O6—Fe1—O7	87.1 (2)
O4—C7	1.234 (8)	O6—Fe1—N1	91.4 (2)
C1—N1	1.346 (10)	N1—Fe1—O1	75.2 (3)
C1—C2	1.378 (7)	N1—Fe1—O8	150.1 (3)
C1—C6	1.506 (8)	N1—Fe1—O3	74.0 (3)
N1—C5	1.325 (10)	N1—Fe1—O7	150.7 (3)

Table 3. Geometry of hydrogen bonds of complex compound [Fe(dipic)(NO_3)(H_2O)$_2$] (Fig.3).

D-H···A	D-H, Å	H···A, Å	D···A, Å	DHA, angle	Symmetry Code
O5 -- H5A .. O2	0.8600	1.9200	2.708(6)	153.00	1-x, -y,1/2+z
O5 -- H5A .. O7	0.8600	2.5500	3.022(8)	115.00	1/2+x, -y,z
O5 -- H5B .. O8	0.8600	2.6000	2.876(7)	100.00	-

O5 -- H5B .. O1	0.8600	1.9000	2.747(7)	173.00	1/2+x, -y,z
O6 -- H6A .. O4	0.8500	1.8700	2.707(6)	168.00	1-x,1-y, -1/2+z
O6 -- H6B .. O3	0.8500	2.0000	2.750(7)	146.00	1/2+x,1-y, z
O6 -- H6B .. O8	0.8500	2.3100	3.002(8)	139.00	1/2+x,1-y, z
C3 -- H3 .. O9	0.9300	2.2200	3.145(6)	179.00	-1+x, y,z

DFT Calculations. To identify the most stable spin state of the Fe(III) complex, density functional theory (DFT) calculations were performed for the doublet, quartet, and sextet spin configurations using the PBE-D4/def2-TZVP and B3LYP-D4/def2-TZVP methods. The calculations were based on the molecular geometry obtained from single-crystal X-ray diffraction analysis. The calculated total energies indicated that the sextet spin state is the most energetically favorable configuration for the Fe(III) complex according to both computational methods.

Table 4. ESP calculation of the Fe complex in different spin-electronic states

Method	Doublet	Quartet	Sextet
PBE-D4/def2-TZVP	-1455925.85	-1455930.00	-1455937.84
B3LYP-D4/def2-TZVP	-1456403.67	-1456406.98	-1456431.57

MO energies and ESP level analyses of this complex sextet state were performed.

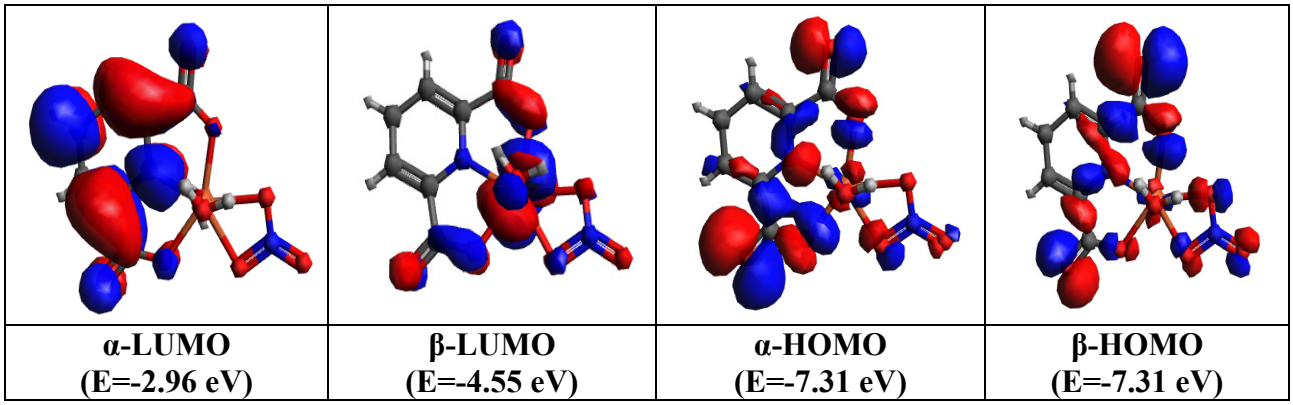


Fig. 4. Frontier molecular orbitals (HOMO and LUMO) and electron density distribution of the [Fe(dipic)(NO_3)(H_2O)$_2$] complex.

Table 5. MO energies and the energy gap (ΔE) of Fe complex in triplet state by PBE-D4/def2-TZVP and B3LYP-D4/ def2-TZVP

	PBE-D4/def2-TZVP					
	HOMO (α)	HOMO(β)	LUMO (α)	LUMO (β)	ΔE(α)	ΔE(β)
Fe complex MO	-5.79	-6.05	-3.61	-5.47	2.18	0.58
The percentage of p and d in the cited MOs (%):	p: 77.23 d: 18.60	p: 94.34 d: 4.90	p: 92.13 d: 7.29	p: 12.79 d: 86.84		
B3LYP-D4/ def2-TZVP						
Fe complex MO	HOMO (α)	HOMO(β)	LUMO (α)	LUMO (β)	ΔE(α)	ΔE(β)

	-7.31	-7.31	-2.96	-4.55	4.35	2.76
The percentage of p and d in the cited MOs (%):	p: 89.00 d: 7.61	p: 94.29 d: 4.88	p: 92.13 d: 7.27	p: 13.50 d: 86.18		

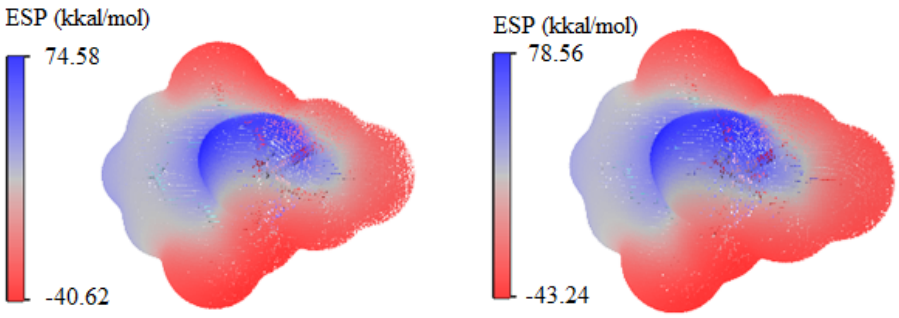


Fig.5. ESP level maxima and minima. PBE (left) and B3LYP (right)

ESP Surface Analysis. Electrostatic potential (ESP) surface analysis is a powerful tool for identifying electron-rich and electron-deficient regions within a molecule. The ESP surface of the investigated complex is shown in Fig. 5. On the ESP map, blue regions correspond to positive potential maxima and represent electron-deficient sites that are susceptible to nucleophilic attack. In contrast, red regions correspond to negative potential minima and indicate electron-rich areas with a high electron density. Therefore, the ESP surface provides valuable information about the distribution of charge and the potential reactive sites of the complex.

The electrostatic potential maxima and minima of the [Fe(dipic)(NO_3)(H_2O)$_2$] complex were evaluated using the PBE-D4/def2-TZVP and B3LYP-D4/def2-TZVP methods. The most positive ESP region is located in the vicinity of the hydrogen atoms of the ligand framework (Fig. 5a,b), with potential values of 74.58 and 78.56 kcal mol^{-1}, respectively. In contrast, the most negative ESP region is localized around the oxygen atoms of the coordinated nitrate group, with potential values of −40.62 and −43.24 kcal mol^{-1}, respectively. These results indicate that the hydrogen atoms act as electron-deficient sites, whereas the nitrate oxygen atoms represent the most electron-rich regions of the complex.

Hirshfeld Surface Analysis. Hirshfeld surface analysis is a valuable tool for investigating weak intermolecular interactions in crystalline materials. It provides insight into both short- and long-range contacts and enables visualization of intermolecular interactions relative to the van der Waals radii of the constituent atoms. The Hirshfeld surface of the [Fe(dipic)(NO_3)(H_2O)$_2$] complex was analyzed using the CrystalExplorer program. The crystal structure is stabilized by C–H···O and O–H···O intermolecular hydrogen bonds. These interactions are represented by distinct red regions on the dnorm-mapped Hirshfeld surface, indicating close intermolecular contacts and significant contributions to the stabilization of the crystal packing.

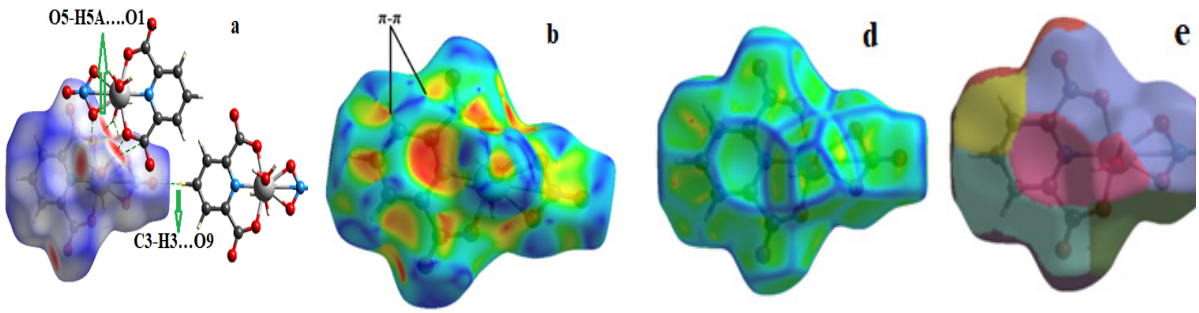


Fig. 6. Hirshfeld surface (a), shape index(*b*), curvedness (*d*) and fragment patches(*e*).

The dnorm-mapped Hirshfeld surface exhibits minimum and maximum values of −0.6743 and 1.0475, respectively. On the dnorm surface, red regions correspond to intermolecular contacts shorter

than the sum of the van der Waals radii, whereas blue regions represent contacts longer than the corresponding van der Waals separations. As shown in Fig. 6, the most prominent red regions are associated with O–H···O and C–H···O hydrogen-bonding interactions, indicating their significant contribution to crystal stabilization.

The Hirshfeld surface area and volume were calculated to be 246.28 Å² and 256.00 Å³, respectively. Quantitative analysis of intermolecular contacts was performed using the two-dimensional fingerprint plots based on the internal (di) and external (de) distances from the Hirshfeld surface. The dominant intermolecular interactions are O···H/H···O contacts, contributing 50.0% of the total surface area, followed by O···C/C···O (19.0%) and H···H (14.4%) interactions (Fig. 7).

Crystal Packing and Void Analysis. The crystal packing and void characteristics of the coordination compound [Fe(dipic)(NO_3)(H_2O)$_2$] were analyzed using the CrystalExplorer program to evaluate the packing efficiency and distribution of unoccupied space within the crystal lattice. Void calculations were performed using a probe radius of 1.2 Å and a grid spacing of 0.2 Å. The complex crystallizes in the orthorhombic crystal system with the space group $Pca2_1$ and a unit-cell volume of 1047.10(3) Å³.

The void analysis revealed a total void volume of 81.04 Å³, corresponding to 12.92% of the unit-cell volume, whereas the remaining 87.08% is occupied by molecular fragments. This relatively low void fraction indicates efficient crystal packing and a densely organized crystal lattice. The absence of large cavities or solvent-accessible channels suggests that the inclusion of guest molecules within the crystal structure is unlikely.

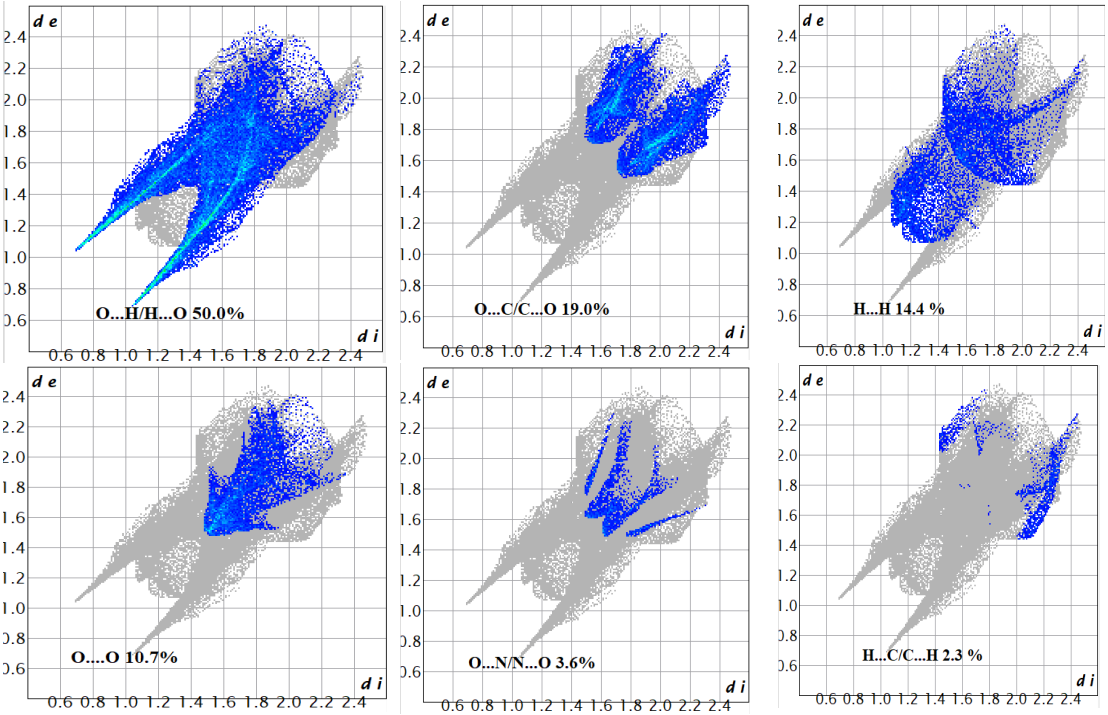
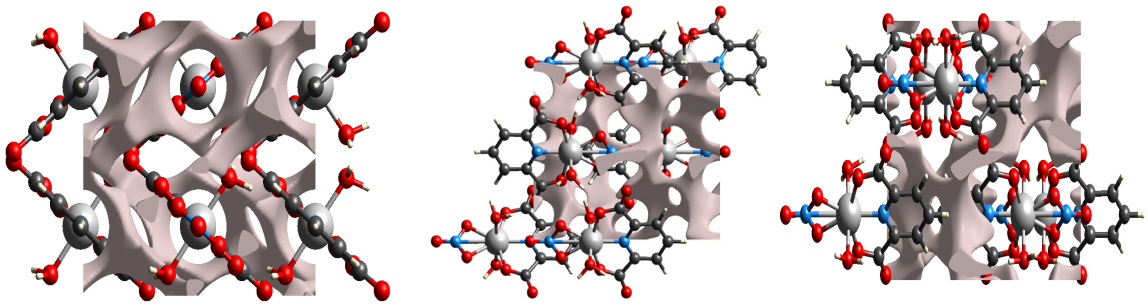


Fig. 7. Two-dimensional (2D) fingerprint plots derived from the Hirshfeld surface analysis of the [Fe(dipic)(NO_3)(H_2O)$_2$] complex

The compact crystal packing is mainly governed by intermolecular O–H···O hydrogen-bonding interactions involving coordinated water molecules and nitrate oxygen atoms, which contribute significantly to crystal stabilization and lattice cohesion.



a b c

Fig. 8. Void surface visualization of the crystal structure of [Fe(dipic)(NO_3)(H_2O)$_2$] generated using CrystalExplorer (probe radius = 1.2 Å, grid spacing = 0.2 Å), viewed along the a, b, and c crystallographic axes. The transparent regions represent the calculated void spaces within the crystal lattice.

The low void percentage (12.92%) is consistent with efficient packing and good structural stability. The void surfaces visualized along the crystallographic axes appear as isolated regions rather than interconnected channels, confirming the absence of significant porosity within the crystal structure. Overall, the void analysis demonstrates that [Fe(dipic)(NO_3)(H_2O)$_2$] exhibits a densely packed crystal structure characterized by high packing efficiency and limited free volume. The stability of the crystal lattice is governed by the combined effect of intermolecular hydrogen-bonding and π–π stacking interactions, which effectively reduce the void space and reinforce the supramolecular framework.

Conclusion

In this research work, a new complex compound crystal consisting of [Fe(dipic)(NO_3)(H_2O)$_2$] was obtained and grown as a single crystal in the presence of Fe(NO_3)$_2$. 6H_2O and 2,6-pyridinedicarboxylic acid. Its structure was confirmed using the X-ray method. Its data were entered into the Cambridge Crystallographic Database (https://www.ccdc.cam.ac.uk/structures/Search?Ccdc=2400919&Author=nazarov&Access=re feree). In order to determine the optimal spin state of Fe(III) of the complex, the doublet, quartet and sextet states of the complex were calculated using the PBE/D4/def2-TZVP and B3LYP/D4/def2-TZVP methods based on the geometry determined by the X-ray method. As a result of the calculations, it was determined that the Fe(III) complex has a minimum energy in the sextet state using both methods. According to the ESP analysis of the complexes, the largest maximum is located near the H atoms of the ligand ring, and the lowest minimum is located near the O atoms of the –NO 3 group of the complex. According to the Hirshfeld surface analysis, it was found that the main part of the main interactions of the atoms is O…H/H…O (50.0%) and O…C/C…O 19.0%. The low void percentage (12.92%) is consistent with a structurally robust and thermodynamically stable crystal packing.

Conflict of Interest

The authors declare that they have no known competing financial interests or personal relationships that could have appeared to influence the work reported in this paper.

References

1. Das B., Baruah J.B. Water clusters in mixed ionic complexes with metal dipicolinate anions. *Journal of Molecular Structure*, 2013, **Vol. 1034**, p. 144–151. DOI:10.1016/j.molstruc.2012.08.046.

2. Sun Y.S., Zhao Z., Yang Z.N., Xu F., Lu H.J., Zhu Z.Y., Shi W., Jiang J., Yao P.P., Zhu H.P. Risk factors and preventions of breast cancer. *International Journal of Biological Sciences*, 2017, **Vol. 13(11),** p. 1387–1397. DOI:10.7150/ijbs.21635.
3. Zhao G., Feng Y., Wen Y. Syntheses, crystal structures and kinetic mechanisms of thermal decomposition of rare earth complexes with Schiff base derived from o-vanillin and p-toluidine. *Journal of Rare Earths*, 2006, **Vol. 24(3),** p. 268–275. DOI:10.1016/S1002-0721(06)60107-5.
4. Alimnazarov B.Kh., Turaev Kh.Kh., Ashurov J.M., Yulchieva M., Suyunov J.R., Rasulov A.A., Shoyimova K. Synthesis and crystal structures of metal complexes of 4-chloro- and 2,4-dichlorophenoxyacetic acid. *Chemical Review and Letters*, 2026, **Vol. 9(2),** p. 286–304. DOI:10.22034/crl.2025.545682.1691.
5. Mirzaei M., Eshtiagh-Hosseini H., Alipour M., Frontera A. On the importance of non-covalent interactions in the structure of coordination Cu(II) and Co(II) complexes of pyrazine- and pyridine-dicarboxylic acid derivatives: Experimental and theoretical views. *CrystEngComm*, 2014, **Vol. 16(27)**, p. 6149–6158. DOI:10.1039/C4CE00331A.
6. Arabieh M., Platas-Iglesias C. A density functional theory study on the interaction of dipicolinic acid with hydrated Fe2+ cation. *Computational and Theoretical Chemistry*, 2016, **Vol. 1090**, p. 134–146. DOI:10.1016/j.comptc.2016.06.010.
7. Razzaqova S.R., Siddique S.A., Todjiyev J.N., Kadirova Sh.A., Rakhmonova D.S., Ibragimov A.B., Normamatov A.S., Ruzmetov A.K., Yakubov Y.Yu., Ibragimov B.T., Balakrishnan C., Abuelizz H.A., Al-Salahi R., Gao J., Bakri Y.E. Synthesis, X-ray Structure Investigation, Hirshfeld Surface Analysis and Theoretical Calculations of Metal Complexes on the Base of 2-Aminobenzoxazole. *Chemistry Select,* 2025, **Vol. 10**, e202500087. DOI:10.1002/slct.202500087
8. Ghasemi F., Ghasemi K., Rezvani A.R., Rosli M.M., Razak I.A. Synthesis, characterization, crystal structure and electrochemical studies of ionic iron(III) dipicolinato complex. *Journal of Molecular Structure*, 2017, **Vol. 1144**, p. 186–190. DOI:10.1016/j.molstruc.2017.05.044.
9. Ilkimen H., Yenikaya C., Dal H., Tunca E., Büyükgüngör O. Synthesis and characterization of a novel proton salt of 2-amino-6-nitrobenzothiazole with 2,6-pyridinedicarboxylic acid and its metal complexes and their antimicrobial and antifungal activity studies. *Journal of Molecular Structure*, 2016, **Vol. 1120**, p. 25–33. DOI:10.1016/j.molstruc.2016.04.068.
10. Ghasemi K., Ghasemi F., Rezvani A.R., Rosli M.M., Razak I.A. Potential antidiabetic drug involving a zinc anionic complex of dipic and metformin as counter ions: Synthesis, characterization, crystal structure and electrochemical studies. *Journal of Molecular Structure*, 2014, **Vol. 1074**, p. 79–84. DOI:10.1016/j.molstruc.2014.05.048.
11. Ghasemi K., Ghasemi F., Rezvani A.R., Rosli M.M., Razak I.A. Mn(II) and Zn(II) ions catalytic oxidation of o-phenylenediamine and characterization, X-ray crystal structure and solution study of the final products DAPH+Cl−·3H_2O and [DAPH][Zn(dipicH)(dipic)]·4H_2O. *Polyhedron*, 2016, **Vol. 110**, p. 55–62. DOI:10.1016/j.poly.2016.02.005.
12. Hojnik N., Kristl M., Golobič A., Turel I. Hydrolytic synthesis of novel lanthanide(III) complexes with pyridine-2,6-dicarboxylic acid: Characterization of the structure and the physical properties. *Journal of Molecular Structure*, 2015, **Vol. 1079**, p. 54–60. DOI:10.1016/j.molstruc.2014.09.029.
13. Ghasemi K., Ghasemi F., Rezvani A.R., Rosli M.M., Razak I.A. A proton transfer and a cobalt(II) compound including 2,6-pyridinedicarboxylate and o-phenylenediamine ions: Synthesis, characterization, crystal structure and solution study. *Comptes Rendus Chimie*, 2014, **Vol. 17(12),** p. 1221–1229. DOI:10.1016/j.crci.2014.03.009.
14. Park H., Kim H., Lee U., Kim C. Different coordination modes of Hdipic and dipic ligands to nickel(II) ions in the same environment (dipic = 2,6-pyridinedicarboxylate, dipicolinate). *Inorganica Chimica Acta*, 2007, **Vol. 360(8),** p. 2819–2823. DOI:10.1016/j.ica.2006.12.047.
15. Moghimi A., Aghabozorg H., Ghasemikhani M., Sheshmani S. A ternary tetracoordinated Pd(II) complex with metformin and dipicolinate: Synthesis, characterization and crystal structure. *Journal of Molecular Structure*, 2011, **Vol. 996(3**), p. 38–41. DOI:10.1016/j.molstruc.2011.03.061.

16. Ghasemi K., Ghasemi F., Rezvani A.R., Rosli M.M., Razak I.A. Chromium(III) complex obtained from dipicolinic acid: Synthesis, characterization, X-ray crystal structure and electrochemical studies. *Bulletin of the Korean Chemical Society*, 2013, **Vol. 34(10),** p. 3093–3097. DOI:10.5012/bkcs.2013.34.10.3093.
17. Prasad T.K., Rajasekharan M.V. [M(dipicH2)(H2O)3]2+, M = Ni, Cu, Zn (dipicH2 = dipicolinic acid): A combined crystallographic, spectroscopic and computational study. *Polyhedron*, 2007, **Vol. 26(7),** p. 1364–1372. DOI:10.1016/j.poly.2006.11.029.
18. Ghosh S.K., Ribas J., Bharadwaj P.K. Metal-organic framework structures of Cu(II) with pyridine-2,6-dicarboxylate and different spacers: Identification of a metal-bound acyclic water tetramer. *CrystEngComm*, 2004, **Vol. 6(45),** p. 250–256. DOI:10.1039/B407571D.
19. Aghajani Z., Sharif M.A., Aghabozorg H., Naderpour A. Bis(2,4,6-triamino-1,3,5-triazin-1-ium) bis(pyridine-2,6-dicarboxylato)zincate(II) decahydrate. *Acta Crystallographica Section E: Structure Reports Online*, 2006, **Vol. 62(4)**, p. m830–m832. DOI:10.1107/S1600536806009688.
20. Tabatabaee M., Dadkhodaee M., Kukovec B.-M. Different coordination environments of iron(III) and pseudopolymorphism in complexes with dipicolinic acid and 2-amino-6-picoline: The influence of molar ratio and solvent type. *Polyhedron*, 2013, **Vol. 51**, p. 316–322. DOI:10.1016/j.poly.2012.12.033.
21. Nomozov A.K., Beknazarov Kh.S., Karimov K.A., Nazarov N.N., Eshkaraev S.S., Umarov Sh.Sh., Ermatova R.O., Shamansurxon T., Beknazarova M.K., Arifdjanova K.S. Synthesis and corrosion inhibition performance of a nitrogen- and phosphorus-containing inhibitor for carbon steel. *Chemical Review and Letters*, 2026, **Vol. 9**, p. 631–639. DOI:10.22034/crl.2026.578785.1805.
22. Morimoto I., Hayashi T., Oida H. The determination of iron with dipicolinic acid. *Nippon Kagaku Zasshi*, 1961, **Vol. 82(2)**, 203. DOI:10.1246/nikkashi1948.82.2_203.
23. Zhang Y., Li B., Ma H., Zhang L., Jiang H., Song H., Zhang L., Luo Y. A nanoscaled lanthanide metal–organic framework as a colorimetric fluorescence sensor for dipicolinic acid based on modulating energy transfer. *Journal of Materials Chemistry C*, 2016, **Vol. 4**, p. 7294–7301. DOI:10.1039/C6TC01022A.
24. Todjiev J., Turaeva G., Turabov N., Jumaev J., Khusanov B., Fuzaylova F., Sapaev I., Tursunqulov J., Mamatkulov N., Razzokova S., Yuldasheva U., Zokirova N., Xazratkulova S., Mukhammadieva D. Trends and developments in extractive spectrophotometric determination of Fe(III), Co(II), and Ni(II): From classical reagents to modern analytical systems. *Chemical Review and Letters*, 2026, **Vol. 9**, p. 877–900. DOI:10.22034/crl.2026.577799.1797.
25. Wang B., Xia J., Zhou G., Li X., Dai M., Jiang D., Li Q. Tb(III)-doped nanosheets as a fluorescent probe for the detection of dipicolinic acid. *RSC Advances*, 2020, **Vol. 10(61)**, p. 37500–37506. DOI:10.1039/C9RA09695G.
26. Ma Y., Yang X., Hao W., Zhu T., Wang C., Schipper D. Ratiometric fluorescent detection of dipicolinic acid as an anthrax biomarker based on a high-nuclearity Yb18 nanoring. *Dalton Transactions*, 2021, **Vol. 50(38)**, p. 13528–13532. DOI:10.1039/D1DT01731D.
27. Yadav U., Abbas Z., Butcher R.J., Patra A.K. A luminescent terbium(III) probe as an efficient "Turn-ON" sensor for dipicolinic acid, a Bacillus anthracis biomarker. *New Journal of Chemistry*, 2022, **Vol. 46(38)**, p. 18285–18294. DOI:10.1039/D2NJ03437A.
28. Gong T., Yang S., Wang Z., Li M., Zhang S., Liu J., Chen L., Zhao J. Dual-ligand-functionalized dodeca-nuclear lanthanide–tungsten-cluster incorporated selenotungstates and fluorescence detection of dipicolinic acid (an anthrax biomarker). *Inorganic Chemistry Frontiers*, 2023, **Vol. 10**, p. 2799–2810. DOI:10.1039/D3QI00361B.
29. Hasanov Kh.I., Azizova A.N., Kulieva N.M., Adjalova G.I., Yusifova M.Yu., Kasumov Sh.G. Membrane-protective properties of palladium(II) complexes containing antioxidant fragment as potential radioprotective agents. *Chemical Problems*, 2025, **Vol. 23(2)**, p. 214–220. DOI:10.32737/2221-8688-2025-2-214-220.
30. Mohammed E.H., AlSultan M., Alasalli S.M., Sabah A.A. Syntheses, characterization and thermal stability study of new Co(II), Cu(II) and Zn(II) complexes derived from Schiff base 4-

(dimethylamino)benzaldehyde. *Chemical Problems*, 2025, **Vol. 23(3),** p. 395–407. DOI:10.32737/2221-8688-2025-3-395-407.